Full length article

Dynamics of body kinematics of freely flying houseflies responding to air turbulence

Nazri Nasir[a,*], Fritz-Olaf Lehmann[b], Peter Schützner[b], Shabudin Mat[a], N.A.R. Nik Mohd[a]

[a] Department of Aeronautics, Automotive and Ocean Engineering, School of Mechanical Engineering, Universiti Teknologi Malaysia, 81310 Skudai, Johor, Malaysia
[b] Institute of Neurobiology, BioFuture Research Group, University of Ulm, 89081 Ulm, Germany

A B S T R A C T

From the world's tiny flying bugs to gigantic dobsonflies, inflight locomotion of a flying creature requires complex biomechanical strategies to cope with air turbulence. These unpredictable changes in ambient airflow strength and direction may destabilize body posture and orientation. To record this behaviour in further detail, we scientifically examined how houseflies (*Musca domestica*) respond to air turbulence. We then, three-dimensionally reconstructed body and wings motion of continuously perturbated houseflies using high-speed videography under laboratory condition. The findings confirmed that houseflies, in general, do not initiate flight when average ambient air speed exceeds $\sim 0.63 \, \text{ms}^{-1}$ at approximately $\sim 2\%$ of relative turbulent intensity. This finding contrasts with flies which immediately take-off after being released. During mild turbulent conditions, flies performed take-off but with severe and active modulation of body postures. In addition, the body roll angle fluctuates more severely (18.5-fold increase) compared to yaw (7-fold of increment) and pitch (6.4-fold of increment) during turbulence, highlighting that body roll stability is highly sensitive. This research extends our current knowledge on flies' behaviours during turbulence and how insects achieve their superior flight performance.

Introduction

Every flying insect has specific habitat preferences. Abiotic condition, parasitism and resource availability are significant preferences, influenced by environmental factors and competitive interaction (Ricklefs and Miller, 1999; Khelifa et al., 2013). Airflow is an important environmental factor that affects the selection of their habitats, emergence sites, spatial distribution and population density (Murty et al., 2010). Turbulence is an unsteady, disorderly structure of airflow in the aerosphere which diversely fluctuates in terms of pressure and velocity (White, 2006). In flying insects, turbulence not only due to environmental factors or meteorological effects but also due to [recaptured wake during flying (Wang et al., 2003), vortex shedding during flapping (Ellington et al., 1996), rotational circulation (Dickinson et al., 1999), and wake structure from adjacent peers (Weimerskirch et al., 2001)]. As the turbulence intensities vary, the mean wind speed, temporal scale, spatial scale and wake region also differ (Combes and Dudley, 2009).

An experimental study showed that walking fruit flies exhibit rapid arrest during a windy environment, which perhaps indicates the adaptation behaviour prior to take-off (Yorozu et al., 2009). Scientific

evidences also found that strong turbulence winds damage insects' soft wings due to structural stress (Purse and Thompson, 2003; Pass, 2018). In addition, the turbulence which surpasses insect flight speed will gradually impair insect stability, thus demanding rigorous deployment of the flight control system as well as limits the duration of mobility (Stuart, 1958). The previous study also disclosed that orchid bees ceased flying and crashed when flight speeds beyond $5.32 \pm 0.57 \, \text{ms}^{-1}$ due to high turbulence strength, including excessive pressure drag (Combes and Dudley, 2009).

Stable flight demands a set of continuous adjustments of wing motion to cope with flight instability that might reduce flight qualities and performance. In insects, aerodynamic forces are produced not only to compensate for body mass but also to cope with instabilities due to changing airflows in their flight apparatus (Dudley, 2002). The control mechanisms correct the unintended body moments and compensate flight heading, which include the changes in non-symmetrical wingbeat amplitude and flapping frequency (Lehmann and Dickinson, 1998), the adjustment of the timing and speed of non-symmetrical wing angle of attack (Faruque and Humbert, 2010) and change in flapping phase between fore and hind-wing in four-winged fliers (Berger and Kutsch, 2003). Surprisingly, to cope with aerial perturbation, these flying

---

creatures move their limbs dynamically [such as birds (Pennycuick, 1960; Pennycuick, 1968), gliding ants (Yanoviak et al., 2010), crickets (Combes and Dudley, 2009), bees (Combes and Dudley, 2009) and fruitflies (Berthé and Lehmann, 2015)] and deploy the abdomen as a control system (Dickerson et al., 2014).

Measuring miniaturized insect behaviour in free-flight by videography is challenging because of fast flight speeds, small body size, rapid changes in body postures, and structural deformations especially wing [e.g. spanwise bending (Mountcastle and Daniel, 2009; Lehmann et al., 2011), wing torsion (Ennos, 1995) and cambering (Ennos, 1988)]. These problems can be solved by numerous techniques, which depend on the experimental conditions. The simplest approach consists of integrated mirrors and a single camera to capture multiple perspectives (Bomphrey et al., 2009). More advanced approaches use two or more high-speed cameras to allow three-dimensional (3D) kinematic reconstruction as listed: (i) the model-based approach, and (2) the reconstruction-based approach.

In this paper, we investigate the responses of flying houseflies' behaviours during turbulence under a controlled laboratory condition. By using a high-speed video apparatus and reconstruction-based approach, we recorded flight sequences and analysed how flies control their body motion to diminish the effect of turbulence airflow. This study provides a videography approach for both entomologists and engineers interested in fast freely moving insects and their behavioural relationship to the environment particularly, with surrounding airflow.

Materials and methods

Animal

In each trial, we tested only female wild-type *Musca domestica* Linnaeus (Insecta: Diptera: Muscidae), commonly known as houseflies aged 5–10 days (Fig. 1). We kept the flies at the Institute of Neurobiology, Faculty of Natural Sciences, University of Ulm, Germany. Nearly 40–50 houseflies were reared inside a transparent glass aquarium (50 cm × 30 cm × 30 cm) with sugar and water as their food, on a 16(light):8(dark) hour of daily routine. All flies are shown to scale by a microgram balance (AT21, Mettler Toledo GmbH, Switzerland). The body, m_b (*see the list of symbols for the definition*) was approximately 18.4 ± 2.0 mg (mean ± s.d., $N = 10$ flies) and freshly cut wing, m_w weighted as 8.3 ± 52.3 μg (mean ± s.d., N = 10 flies, in total 20

wings for both left and right sides). Body length, l_b was 9.62 ± 0.02 mm and wing length, l_w 6.98 ± 0.03 mm (mean ± s.d., $N = 10$ flies, in total 20 wings for both left and right sides). To attract and further capture flyable individuals, we used a white light trap (10 cm length with a 4 cm diameter Plexiglas cylinder) mounted at the upper part of the aquarium.

Marking procedure

The flies slept for 5 minutes on ice flakes before we painted the bodies and wings with fluorescent spots (Pedeko, Monchengladbach, Germany; Fig. 1C). It took 5 minutes and every fluorescent spot had a mass of 0.1 μg to avoid structural flexing, especially wings, owing to inertia. The typical size of the fluorescent spot was 0.25 mm in diameter (2–3 image pixels). Due to inertia, the mean wing beat amplitude increased only 1.6% compared to unmarked flies, which is not significantly different (unmarked: 147.5 ± 14.6°, marked: 149.9 ± 9.8°, two sample unpaired *t*-test, $P < .05$, N = 10) (Schützner, 2016). After that, we placed the flies on the take-off stage and they were allowed to recover (Fig. 2A).

Videography

To film the fluorescent markers, we built a modified experimental setup similar to the previously used approaches using master-slave configuration. The experimental setup comprises three high-speed cameras (Phantom v12, 1280 × 800-pixel, 6000 fps, Vision Research Inc., NJ, USA; Fig. 2) and calibrated using Direct Linear Transformation, DLT (Abdel-Aziz and Karara, 1971). At 170 Hz flapping frequency, this resulted in 35 video frames per wing stroke cycle. We mounted the high-speed cameras 18 cm on top of the recording volume that enables us to record the tested flies inside a field of view of 6 cm × 5 cm × 5 cm. We fitted each camera with a micro-lens (Nikkor, 60 mm, f/2.8D, Japan) equipped with ultraviolet and red-light filters (Josef Schneider Optische Werke GmbH, Germany) to eliminate any reflected light.

We calibrated the region of interest (ROI) using graph paper that needs to be seen on every camera. There are 25 positions of calibration point in eight different layers of 5 mm equidistant steps in elevation, resulting in 200 positions inside the ROI. We repeated the calibration several times to confirm the high accuracy and consistency.

Airflow condition

The turbulence generator comprises eight computer fans glued together in an octagonal configuration (Fig. 3). Each fan size was 8 cm × 8 cm × 2.5 cm (height × width × thickness) (model

A Lateral view

B Anterior view

4mm

C Dorsal view

M1 M12 M2 M4 M6 M7 M8 M9 M10 M3 M11 M5
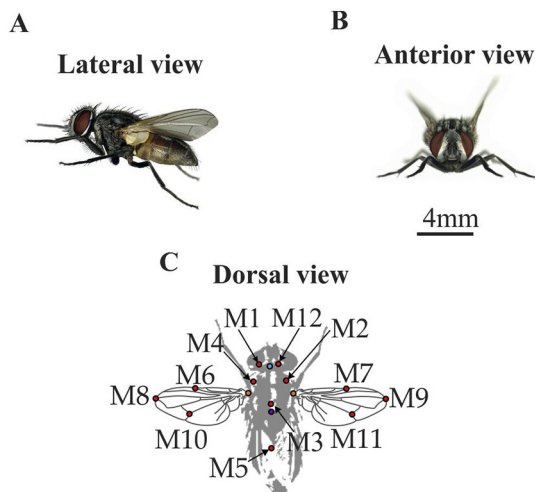
Fig. 1. (**A-B**) Morphology of a housefly (photographed by Hastings et al. 2004). (**C**) The fluorescent dots and virtual points formulated from the form and structure of the housefly are the centre of head rotation (cyan), centre of gravity (purple) and wing hinges (orange). (For interpretation of the references to colour in this figure legend, the reader is referred to the web version of this article.)

A Side view

Cameras
Guidance light and phototransistor
Ultraviolet LEDs
Infra-red laser trigger
Take-off platform
Z → Y

B Top view

UV LEDs flashers
Slave camera 2
120°
Master camera
120°
120°
Slave camera 1
Take-off platform
X → Y
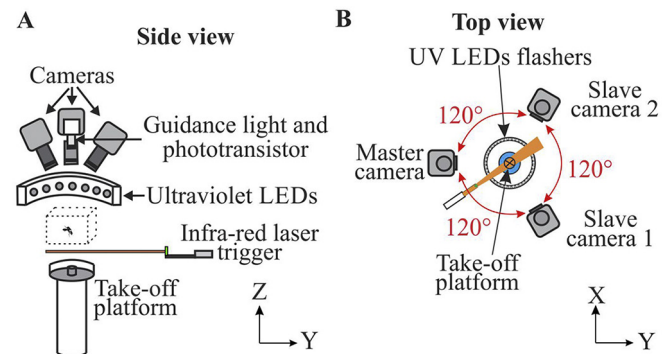
Fig. 2. Experimental setup of 3D-videography to film flight of flying flies. The high-speed cameras and UV flashers placed above the Region of Interest (a volume with dashed lines). White guidance LEDs light provides visual guidance (5 mm diameter, Cree, NC, US).
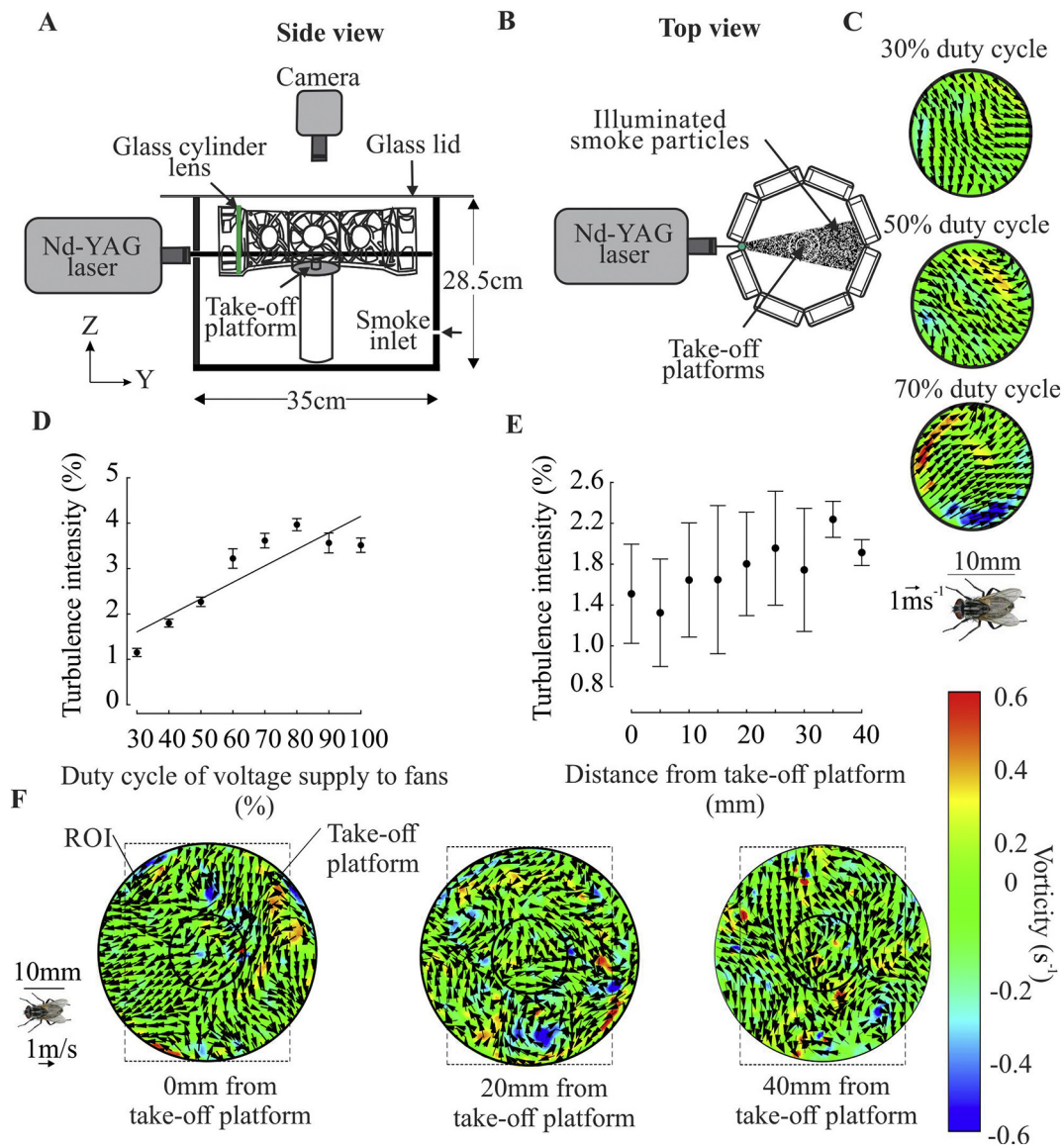
Fig. 3. Experimental setup to quantify turbulence airflow using Digital Particle Image Velocimetry (DPIV). (**A**) A laser illuminated smoke particles, recorded by a high-speed camera above a black painted wooden box. (**B**) Top view of the experimental setup. (**C**) Change of flow characteristics with fan speed at 5 mm above the take-off platform. Airflow velocity vectors and average vorticity contours at 30%, 50%, and 70% duty cycles of voltage supply to the fans. (**D**) Mean turbulence intensity at various duty cycles of voltage supply to the fans (**E**) Mean turbulence intensity at various heights above take-off platform. (**F**) Flow characteristics of turbulent flow above take-off platform at 37% duty cycle of voltage supply to the fans. Snapshot of mean air velocity and mean vorticity at 0 mm, 20 mm and 40 mm above the platform. Dashed lines indicate the region of interest. The fly is shown for size comparison. The fly is shown for size comparison. $N = 50$ measurements.

KDE1208PTV1, DC1 2 V/1.6 W, Sunon Maglev, CA, US) and connected to a duty cycle controller, regulated by a waveform generator (Model WG8100, Tektronix, OR, USA). The region of interest at the centre of the arena was 6 cm × 6 cm × 6 cm (height × width × thickness).

To characterize the turbulent airflow, we performed Digital Particle Image Velocimetry (DPIV), without the flies. We used smoke seeding particles inside a black container sized 35.5 cm × 35.5 cm × 28.5 cm. It was then sheltered by a transparent lid. The smoke particles were sized 90 μm diameter and ignited by matches (Splintax, Raketenmobellbau Klima GmbH, Emersacker, Germany). We also used a dual mini Nd:YAG laser (50 mJ per pulse, Solo III, Insight v5.1, Shoreview, MN, USA) to create 2 similar light sheets, which separated in time by 250 ms (Δt). A glass cylinder (3 mm diameter) placed between two fans transformed the laser beams into a horizontal light sheet (5 mm thickness). A 155 cm^2 flow field of paired images were recorded using a camera (2 M high-definition, model 630057, PowerView, TSI, MN, USA) at a filming frequency of 14.5 Hz. In order to determine the displacement directions

and magnitude of the particle, the frames were cross-correlated by a Fast Fourier Transform (FFT) with an area of 32 pixels × 32 pixels. All 50 paired airflow images were quantified in a region of interest sized 55 mm diameter (area, 38×10^{-3} m^2) using Insight 3G™ v10.3.0 (TSI Inc., St Paul, MN, USA). The vectors were then smoothed by a low-pass filter in a 3 × 3 grid. After that, we calculated the local speed, vorticity (local rotational motion) and turbulence intensity (total standard deviation of velocity vectors) using Tecplot 360 v2013R1 (WA, USA). However, this experimental setup has limited recording speed, which did not allow us to estimate the change in airflow within the fly stroke cycle (170 Hz of flapping frequency). The DPIV has only analysed the horizontal airflow because each fan produced the symmetrical airjet. An issue that was not addressed in this study is whether the neighbouring airjet will affect the symmetrical airflow because the arrangement of the experimental setup did not allow us to acknowledge this issue further.

The characteristics of the airflow field on the take-off platform vary

with the elevating fan speed. The average for all 6197 vectors of airflow field indicate that the rise of fans speed led to an increase in airspeed (ANOVA, $F_{7,49,747} = 1176.8$, $p < 0.001$, fitting-line equation: $y = 0.01\times + 0.17, r = 0.90, p < 0.01$) and turbulence intensity (Kruskal-Wallis test, Chi-square value $= 386.43$, p < .001, fitting-line equation: $y = 36.36 \times 10^{-3}x + 514.65 \times 10^{-3}, r = 0.88$, p < 0.01; Fig. 3D). The airspeed rise with the increasing duty cycle of the voltage supply ($u_{a,DC=30} = 0.36 \, ms^{-1} \pm 0.22 \, ms^{-1}$, $u_{a,DC=50} = 0.74 \pm 0.40 \, ms^{-1}$, $u_{a,DC=70} = 1.09 \pm 0.72 \, ms^{-1}$), however, the relationship of fan speed and vorticity remains indistinct (ANOVA of airspeed, $F_{7,400} = 0.4535$, $p > 0.05$). The duty cycle of the voltage supply is a proportion between the time when voltage is active and total period. The existence of vortex structures (Fig. 3C at 70% duty cycle) confirms the high intensity of turbulence airflow filled in the testing volume. The result also shows that airspeed expressively rises with the increasing of upright height from the take-off platform (ANOVA, fitting-line equation: $y = 7.84 \times 10^{-3}x + 457 \times 10^{-3}$, $r = 0.83$, $p < 0.05$, $N = 9$ data points). In the meantime, turbulence intensity linearly rises with the increasing height of measurement plane (fitting-line equation: $y = 0.016\times + 1.43$, r = 0.83, p < .05, N = 9 data points, Fig. 3E). Nevertheless, the airflow vorticity was independent of the upright height of the take-off platform. (ANOVA, $F_{8,441} = 6.39$, p < 0.05).

Ultraviolet light flasher

To reduce motion blur of fluorescent markers, a ring of 40 UV LEDs (405 nm wavelength, 3 mm diameter, 20° viewing angle, 40mWsr^{-1} radiant intensity, Bivar, CA, US) flashers were illuminated with l60 µs of pulses and as well as synchronized with cameras (Fig. 2). This arrangement distributed ultraviolet light (9 ± 5% lux) to each direction, which is likely to record the housefly, especially during extreme manoeuvres. Although ultraviolet light illumination led to degradation of steering performance, flies still accomplished the assigned visual task during flight (Lehmann et al., 2013).

Optical detection system

Next, we prepared a detection system to trigger the cameras automatically (Fig. 2a). We constructed a horizontally oriented 2 mm thickness infrared (IR) light sheet (QL8516SA, 850 nm wavelength, 60° opening angle, 30 mW, Roithner Lasertechnik GmbH, Vienna, Austria). At the same time, a phototransistor (L-53P3C, Kingbright, Taiwan) was installed above the recording arena sensed changes in laser light when a housefly passed the laser sheet. A charge-coupled device (CCD) zoom lens (TF15DA-8, f/2.2 fixed focal length manual Iris C-mount, Fujinon, Tokyo, Japan) equipped with an 830 nm IR filter (R-72, Heliopan Lichtfilter-Technik Summer GmbH and Co. KG, Munich, Germany) was equipped in front of the phototransistor's casing. If a tested fly passed the IR sheet, the phototransistor which linked to a switching circuit, generated a 5 V Time-to-live (TTL) signal to an acquisition system (NI USB 6009, 14 Bits, 48 kS/s, National Instruments, TX, USA) and eventually triggered the high-speed camera. Housefly's photoreceptors could not sense the IR light because the visual ability ranges only from 380 to 600 nm of light wavelength (Stark and Johnson, 1980).

Image processing and three-dimensional reconstruction

To eliminate noises and improve image quality, we used the VirtualDub v1.9.9 ([31]. The image processing tool stretched the brightness level ([0.00–0.023] > 2.01 > [0.00–1.00] (Y)), 400% of image contrast, and applied box blur (power 2, radius 2). These image-editing processes enhanced the automated tracking routine and kept the search frame at the midpoint of markers.

To track and further digitize the image, we used a MATLAB™ script named DLTdv3 (Hedrick, 2008). This application has a helpful graphical user interface, for example, auto-tracking, zooming and live viewing window of all cameras (Nasir and Mat, 2019). The auto-tracker mode forecasts the position of dedicated markers on next video images by fitting an equation of Kalman filter and extrapolate the location of the marker in the subsequent video image. If the expected marker location matched the auto-track threshold, the tracker continued to digitize the subsequent image. MATLAB uses a minimum of two images and the DLT coefficients to generate the 3D body and wings' motions. In terms of performance, this MATLAB tracking procedure digitized one image in 0.15 s (using a 3.20 GHz Inter® Core™ machine).

Result

Take-off behaviour during continuous perturbation of turbulence

Immediately after the flies left the take-off platform (Fig. 2), flies instantly subjected to turbulence (Duty cycle of the voltage supply to the fans, DT = 30%–100%, turbulence intensity, $I = 0.6\%$–1.87%, mean airspeed, $u_a = 0.47$–1.2 ms^{-1}, $N = 89$ flies). According to the data, control flies (non-perturbated flies which fly at average turbulent airspeed equal to zero) commenced flight straightaway as they reached the take-off platform. In contrast to the perturbated flies, after 30 min, 23.6% of the flies still did not perform take-off, perhaps due to the comparatively high strength of turbulence airflow (red dots, Fig. 4A). This behaviour first began at 0.63 ms^{-1} of transient airspeed and turbulence intensity of ~2%. The take-off delay also significantly increased with higher turbulence airspeed (linear regression fit, $y = 13.21\chi$-4, $r = 0.83$, ANOVA: F = 10, $p = .02$, Fig. 4B). We observed that as the turbulence strength and its intensity increased, flies gripped on the take-off platform longer, which and limited their mobility.

Under turbulence airflow, $u_a = 0.47$–0.77 ms^{-1} (grey region in Fig. 4A), 40 ms after take-off from the platform, flies' three dimensional body positions were -4.9 ± 8.3 mm (x-axis), 5.27 ± 12.3 mm(y-axis), 15.3 ± 7.1 mm(z-axis) ($N = 44$ flies, the second row of Fig. 5). Although, the body scattering of perturbated flies was no significant difference to controls (-6.42 ± 10.3 mm, -1.04 ± 9.1 mm and 13.39 ± 5.2 mm; t-test, $p > .05$; $N = 17$ flies, the first row of. Fig. 5). During turbulence, flies were dispersed in a larger volume. The variance of mean body position, $\sigma_X \times \sigma_Y \times \sigma_Z$ (in standard deviation) in all axes significantly increased over time (linear regression fit, $y = 16.34\times + 12.6$, $r = 0.99$, ANOVA: F = 138.2, $p < .001$, $N = 6$ data points) with 2.2-fold higher rate of increase compared to controls
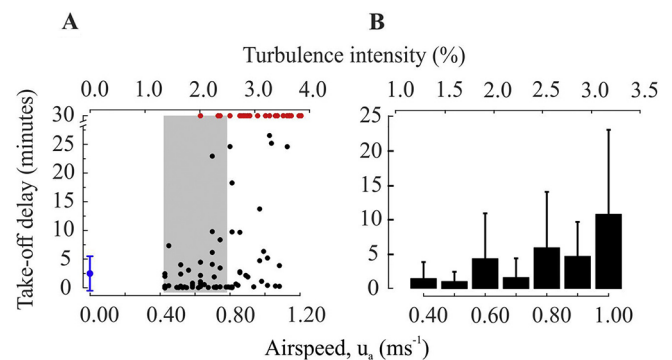
Fig. 4. Time before take-off from the platform plotted as a function of turbulence strengths of continuous perturbation (black dots, $N = 89$ flies). Flies that refused to take-off within < 30 min are shown in red ($N = 23$ flies). Flies that take-off inside in a non-turbulence environment are shown in blue (controls, $N = 17$ flies). Grey area indicates the characteristics of airflow used in the experimental setup for further analysis of body alteration during perturbation ($N = 44$ flies). **(B)** Take-off delay and standard deviation plotted as a function of turbulence strengths (Linear regression fit, $y = 13.21\chi$-4, R2 = 0.69, $p = .02$, $N = 66$ flies). (For interpretation of the references to colour in this figure legend, the reader is referred to the web version of this article.)
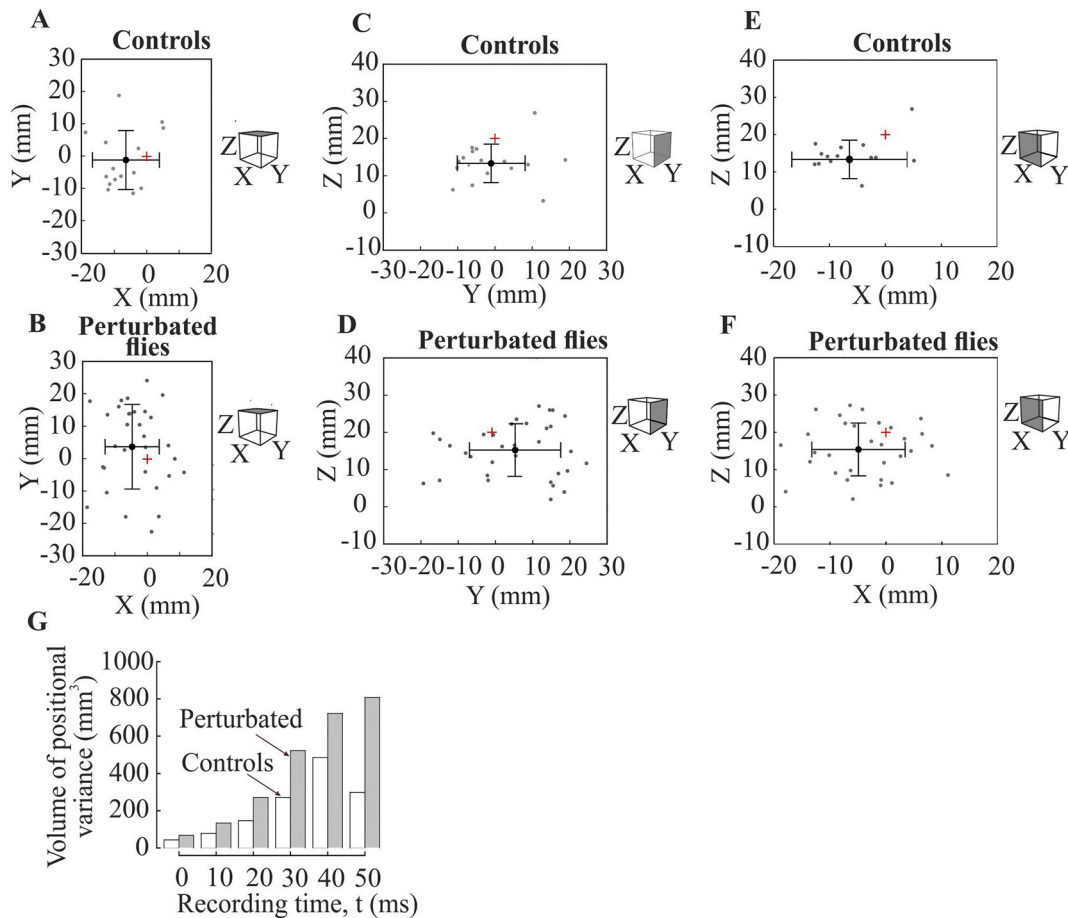
Fig. 5. Flies positions (grey dots) in non-perturbated flows (second row, N = 17 flies) and turbulent flow (first row, N = 44 flies) after 40 ms of video recording. Mean position and standard deviation of each position (X, Y, Z): -6.42 ± 10.3 mm, -1.04 ± 9.1 mm, 13.39 ± 5.17 mm (controls) and -4.9 ± 8.33 mm, 5.27 ± 12.27 mm, 15.32 ± 7.07 mm (perturbated flies). **(A-B)** Top view X-Y axis, **(C-D)** side view Z-Y axis and **(E-F)** side view Z-X axis. Centre of ROI is (0, 0, 20). (G) Volume of positional variance (s.d.X × s.d.Y × s.d.Z) of perturbated flies (grey bar) and controls (white bar).

(linear regression fit, $y = 7.49 \times + 33.25$, $r = 0.85$, ANOVA: F = 10.5, $p = .03$, N = 6 data points). After 40 ms, when flies reached the centre of the cameras' ROI, the volume of positional variance was $723 \, \text{mm}^3$, which is 1.5 times larger than controls ($484.5 \, \text{mm}^3$).

Control experiments

After take-off, control flies flew, on average, with $0.36 \pm 0.1 \, \text{ms}^{-1}$ of vertical translational velocity (Fig. 6B), which is 36.11% higher than horizontal translational velocity ($0.23 \pm 0.1 \, \text{ms}^{-1}$, Fig. 6E, See Supplementary Movie S1). Flies then gradually demonstrated vertical deceleration when they approached a conversion from predominant vertical to horizontal flight manoeuvres. Control flies first initiated flight with body angular velocity as follows ($-15.8 \pm 214.5°\text{s}^{-1}$, roll angular velocity, Fig. 7C; $-37 \pm 209°\text{s}^{-1}$, pitch angular velocity, Fig. 7B; $43 \pm 133°\text{s}^{-1}$, yaw angular velocity, Fig. 7A; N = 32). Flies took-off with an abrupt increase of angular pitch velocity (pitch-up acceleration, $18,378 \pm 89°\text{s}^{-2}$ at $t = -7.4$ ms until 27.4 ms). When flies reached a stable flight condition with predominant horizontal translational motion, we observed that flies gradually decelerated their angular body pitch (nose-down, $-41556 \pm 140°\text{s}^{-2}$, $t = 27.4$ ms until 45.8 ms) probably due to drag acting on the ventral body surfaces. The result indicates that the change in body roll angle was relatively marginal (mean, $7.25 \pm 1.26°$, N = 3027 data points). Thereafter, flies'

responded to aerodynamic perturbations by systematically altering their body yaw, pitch, and roll angular velocity.

Translational velocities

Under moderate turbulent airflow (grey area, Fig. 4A), 94% of the flies took-off steeply within 4.2 ± 8.2 min (mean $\pm$ s.d.) after reached the platform. Flies balanced their bodies in 43 ms, before the fluctuated mean translational velocity continuously dropped (Fig. 6E). Compared to perturbated flies, the control flies reached stable flight conditions 12 ms later (at $t = \sim 55$ ms). This moment is described as predominant vertical flight, which eventually reduced because flight manoeuvres change to horizontal flight (for example forward flight, sideslip or even backward movements). During turbulence, vertical translational velocity demonstrated higher gradual decrease compared to control flies (rate of decrease = $-5.89 \pm 0.02 \, \text{ms}^{-2}$ which started at $t = 62$ ms versus controls, rate of decrease = $-9.33 \pm 0.03 \, \text{ms}^{-2}$ which started at $t = 43$ ms). Despite the perturbated flies altered the vertical translational velocity, the alteration was comparatively small and statistically not significant (t-test, all instantaneous $p > .05$, Fig. 6C, N = 44). An identical trend holds for horizontal translational velocity ($0.24 \pm 0.05 \, \text{ms}^{-1}$, Fig. 6D–E), as the flies have insignificant adjustments compared to controls ($0.23 \pm 0.04 \, \text{ms}^{-1}$, t-test, all instantaneous $p > 0.05$, N = 17, Fig. 6F). Comparing perturbated flies and controls,
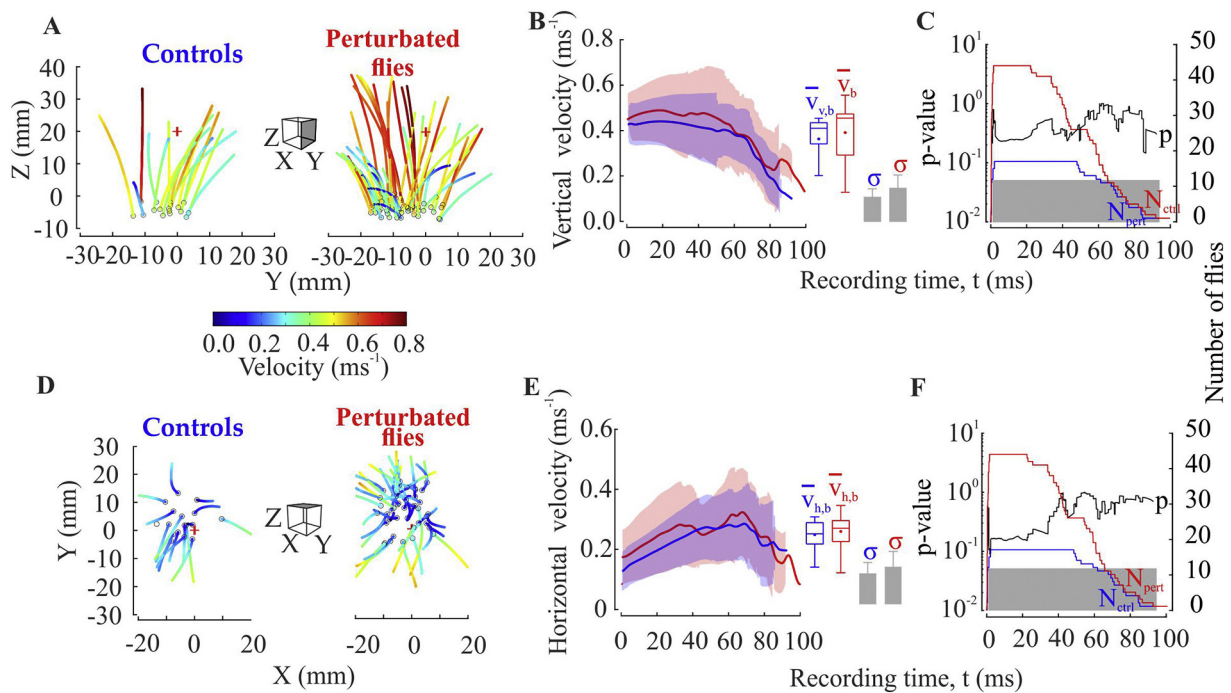
Fig. 6. Alterations in body translational velocity during continuous perturbation (N = 44 flies) compared to controls (blue, N = 17 flies). Velocity in **A** and **D** are plotted in pseudo-colour. Black circles show the time when the fly entered the ROI. (Left column) Flight paths and (middle column) time trace of means and standard deviations (transparent blue for controls and transparent red for perturbated flies). Inset (boxplots and error bars) shows the temporal means of **(B)** vertical translational velocity: 0.36 ± 0.10 ms-1 (controls, blue), 0.39 ± 0.10 ms-1 (perturbated, red) and **(E)** horizontal translational velocity: 0.23 ± 0.04 ms-1 (controls, blue), 0.24 ± 0.05 ms-1 (perturbated, red). (Right column) Statistical comparison (*t*-test) of vertical translational velocity **(C)** and horizontal translational velocity **(F)** of perturbated flies compared to controls. Grey area shows *p*-value of < 0.05. Blue (controls) and red lines (perturbated flies) indicate the number of flies used in the experiment (right scale). (For interpretation of the references to colour in this figure legend, the reader is referred to the web version of this article.)
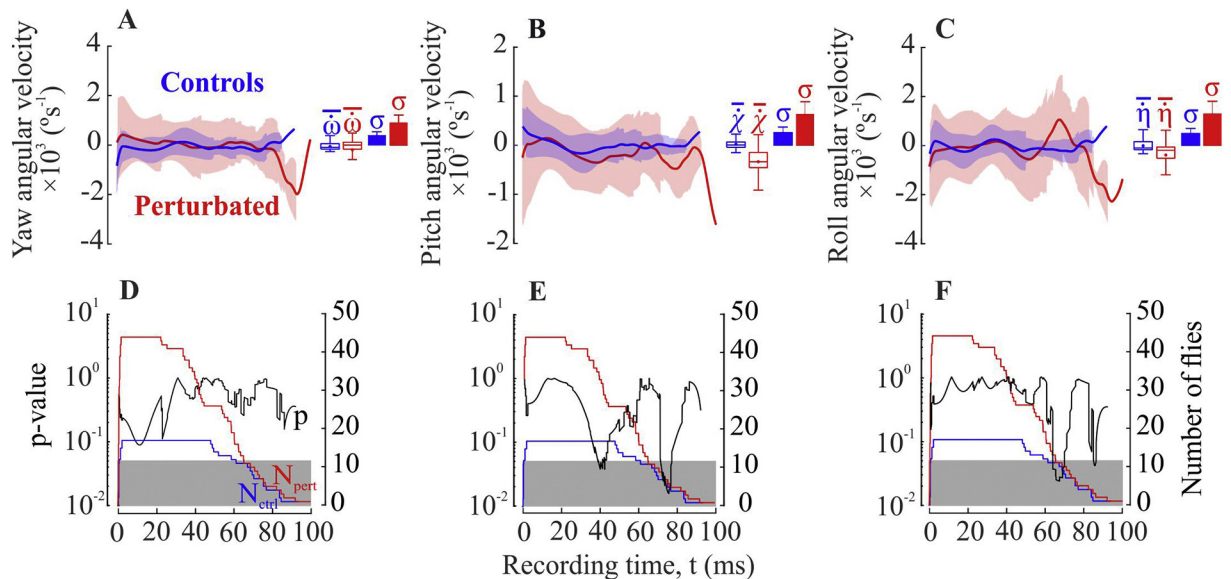
Fig. 7. Body kinematics responding to continuous perturbation (red, N = 44 flies) and controls (blue, N = 17 flies). **(A, B, C)** Time trace of body **(A)** yaw angular velocity, **(B)** pitch angular velocity and **(C)** roll angular velocity. Inset (boxplots and error bars) show mean values, medians and standard deviation of body angular velocity over all data points. **(D, E, F)** Time traces of statistical comparison (*t*-test) between continuously perturbated flies and controls (left scale). Blue (controls) and red lines (perturbated flies) in **C, F** and **I** indicate the number of flies used in experiment (right scale). All positive angular velocities (yaw and roll) indicate clockwise body rotation about their axes except pitch. (For interpretation of the references to colour in this figure legend, the reader is referred to the web version of this article.)

the finding indicates that there are insignificant dissimilarities at any point of 100 ms flight period (*t*-test, all instantaneous p > 0.05). The transition from a predominant vertical to straight flight caused a smoother increase of body horizontal velocity of controls compared to

perturbated flies, which exhibited significant fluctuations (noticeably at *t* = 40 ms). This increasing trend was consistent before horizontal velocity hit maximum point at 68 ms and eventually, both traces of controls and perturbated flies demonstrated prompt reductions.

Angular velocities

During turbulence, the yaw angular velocity of the flies reduced to -188 ± 577°s^{-1} (6.4-times of reduction compared to controls, 43 ± 133°s^{-1}), which was insignificantly changes compared to controls (*t*-test, all instantaneous p > 0.05, Fig. 7A, D). Meanwhile, body pitch and roll angular velocity change considerably during these continuous perturbations compared to controls (Fig. 7E, F). Comparing the controls with perturbated flies, it can be seen that pitch angular velocities of both tested flies were significantly dissimilar (the first alteration occurred 40 ms after take-off and lasted after 3 ms; the second alteration then commenced 72 ms after take-off and lasted after 5.8 ms; *t*-test, all instantaneous $p < .05$, Fig. 7B, E). An equal flight response holds for roll angular velocity, as the first adjustment ensued 64 ms after take-off and ended after 6 ms. After this response, the second alteration happened 85 ms after take-off and eventually ended shortly after 1.3 ms (*t*-test, $p < 0.05$, Fig. 7C, F). In general, after take-off, only 7.3% of instantaneous probability value (*p*-values) for pitch angular velocity and 9% of instantaneous p-values for roll angular velocity were lower than 0.05. During turbulence, overall pitch angular velocity was -261 ± 301°s^{-1} (7-times of decrease compared to controls, -37 ± 209°s^{-1}) and roll angular velocity reduced to -293 ± 760°s^{-1} (18.5-times of decrease compared to controls, -15.8 ± 214.5°s^{-1}). Thus, flies facing turbulence deployed higher alterations of body pitch angular velocity than yaw angular velocity and roll angular velocity.

Discussion

The aim of this study is to quantitatively investigate the behavioural responses of houseflies inside the turbulent flow. To assess the behavioural effects and their relationship to the change of surrounding wind condition, we scored the alterations in body kinematics of freely flying insects.

Preceding studies suggested that the decision to take-off depends on various behavioural and physiological factors [aphids (Dixon and Mercer, 1983); scale insect (Washburn and Washburn, 1984)]. For example, at a wind speed of 0.54 ms^{-1} - 0.67 ms^{-1}, small insects such as aphids may lose body control and blown away. Further studies showed that houseflies also refuse to perform take-off under extremely windy conditions and they inhibit all flight activities (Digby, 1958). By contrast, light wind gust is part of the 'catalyst' or an activating effect for locusts to initiate their aerial activity (Kennedy, 1939). Another example, the flight activity of *Calliphora vicina* (Insecta: Diptera: Calliphoridae) increases with the increasing wind speed up to 0.7 ms^{-1} (Digby, 1958). However, during gustier conditions, these flying insects began to freeze locomotion activity with longer resting periods (> 20 min of latency). There are consistencies between the current study and previous works in the field that can be highlighted. Fig. 4 shows that mean take-off latency linearly increases with increasing turbulence strength (linear regression fit, $y = 13.21\chi\text{-}4$, $R^2 = 0.69$, $p = 0.02$, $N = 66$ flies). We found that at 0.7 ms^{-1} wind speed after flies left the reservoir, they required 4.2 ± 8.2 minutes resting time prior to take-off. By contrast, at the average airspeed of turbulent flow lower than 0.7 ms^{-1}, the probability for flies to perform take-off is relatively high. It can thus be suggested that flies first adapt and gradually exploit the changes of the ambient wind because their motor neurons activities associated with wind speed and direction (Camhi and Hinkle, 1974; Broce et al., 1991). This learning behaviour ensures that their upcoming flight routine is minimally affected (Klassen and Hocking, 1964).

Tiny insects with relatively small flight forces confronts severe catastrophic challenges compared to larger insects (Byrne et al., 1988). Previous data have already shown that ambient flows are used for the dispersion of animals, mostly for food, mating and egg-laying behaviour (Byrne and Bellows, 1991; Withers and Harris, 1997). However, this activity involves a considerable amount of energy expenditure owing to inertia and aerodynamic force production. Despite the small camera's ROI, our data confirmed earlier findings that turbulent environments induced 1.5-fold broader volume of positional variance compared to controls (Fig. 5). Although the average flight trajectories of continuously perturbated flies are not statistically different from controls, the variance of mean body position increased in time (2.2-fold higher rate of increase compared to controls after 50 ms take-off; Fig. 5G). Small insects have tiny wings and their aerial mobility relative to the ground is thought to be mainly dominated by air movement.

The alterations of body angle during aerial perturbation change the inclination angle of the stroke plane and thus alter the direction of mean forces (Vogel, 1966). Therefore, during turbulence, flies will experience continuous body rotational fluctuations compared to controls (Beatus et al., 2015). For example, bees laterally incline their vertical net force, which inherits higher temporal alteration of body roll during upwind turbulence stream (Combes and Dudley, 2009). Under turbulent conditions, our data (Fig. 7) corroborate the earlier studies that body roll angle was primarily affected (18.5-fold increase) compared to pitch (7-fold increase) and yaw (6.4-fold increase). Changes in the standard deviation of body angular velocities as a measure of flight instabilities also indicate that roll is higher than those of pitch and yaw (760°s^{-1} versus 577°s^{-1} for yaw and 301°s^{-1} for pitch). The finding of this research supports the previous study because the roll moment of inertia has the lowest value compared to pitch and yaw (Lin et al., 2012). Therefore, flying insects are highly unstable and face more challenging about roll axis, especially during lateral perturbation [fruit fly (Zhang and Sun, 2010; Beatus et al., 2015), bees (Combes and Dudley, 2009; Ravi et al., 2013; Vance et al., 2013)]. This finding highlights the importance of tracking longer migratory flight trajectories of the small flying migrants, so that drift behaviour due to lateral perturbation (e.g. side or crosswind) can be analysed. Any failure to mitigate crosswind will definitely affect their flying heading vector, which results in a longer duration of flight time to reach the destination.

Supplementary data to this article can be found online at https://doi.org/10.1016/j.aspen.2019.09.002.

List of symbol

α	Angle between the wing chord and vertical axis; wing angle of attack
β	Horizontal deviation angle between flight direction of the fly's centre of gravity and body yaw angle in global co-ordinate frame
ε	Angle between the flight path of an ascending fly and local horizon; body inclination
DLT	Direct Linear Transformation
DT	Duty cycle of the voltage supply to the fans
m	Mass
N	Number of flies
l	Length
n	Wingbeat frequency measured when wing chord was perpendicular to stroke plane
Φ	Stroke angle of the wing with respect to fly's transversal body axis
θ	Elevation angle of the wing with respect to fly's longitudinal body axis
R^2	Coefficient of determination
r	Pearson's correlation coefficient
SSE	Sum of Squared Errors
u	Speed
V	Voltage
v	Velocity
η	Roll angle of the thorax with respect to fly's longitudinal body axis

ω	Yaw angle of fly's longitudinal axis about the vertical
χ	Pitch angle of fly's longitudinal axis with respect to horizon
ROI	Cameras' Region of Interest
s.d.	Standard deviation
$(\ldots)_a$	Airflow
$(\ldots)_b$	Body (Distance between lower ocelli to anus)
$(\ldots)_{h/v}$	Horizontal/ vertical
$(\ldots)_{L/R}$	Left/Right
$(\ldots)_t$	Wingtip
$(\ldots)_w$	Wing (Distance between wing root to wing tip)

Declaration of Competing Interest

None.

Acknowledgements

References

Abdel-Aziz, Y.I., Karara, H.M., 1971. Direct linear transformation into object space co-ordinates in close-range photogrammetry. Symposium on Close-Range Photogrammetry. 1–18.

Beatus, T., Guckenheimer, J.M., Cohen, I., 2015. Controlling roll perturbations in fruit flies. J. R. Soc. Interface 12 (105).

Berger, S., Kutsch, W., 2003. Turning manoeuvres in free-flying locusts: high-speed video-monitoring. J. Exp. Zool. A Comp. Exp. Biol. 299A (2), 127.

Berthé, R., Lehmann, F.-O., 2015. Body appendages fine-tune posture and moments in freely manoeuvring fruit flies. J. Exp. Biol. 218 (20), 3295.

Bomphrey, R., Taylor, G., Thomas, A.R., 2009. Smoke visualization of free-flying bumblebees indicates independent leading-edge vortices on each wing pair. Exp. Fluids 46 (5), 811.

Broce, A.B., Schwenke, J.R., Hampton, K.E., 1991. Landing Pattern of Stable Flies (*Diptera: Muscidae*) on the Alsynite Cylinder Trap: Effect of Wind Speed and Direction.

Byrne, D.N., Bellows, T.S., 1991. Whitefly biology. Annu. Rev. Entomol. 36 (1), 431–457.

Byrne, D.N., Buchmann, S.L., Spangler, H.G., 1988. Relationship between wing loading, Wingbeat frequency and body mass in homopterous insects. J. Exp. Biol. 135 (1), 9.

Camhi, J.M., Hinkle, M., 1974. Response modification by the central flight oscillator of locusts. J. Exp. Biol. 60 (2), 477.

Combes, S.A., Dudley, R., 2009. Turbulence-driven instabilities limit insect flight performance. Proc. Natl. Acad. Sci. U. S. A. 106 (22), 9105.

Dickerson, B.H., Aldworth, Z.N., Daniel, T.L., 2014. Control of moth flight posture is mediated by wing mechanosensory feedback. J. Exp. Biol. 217 (13), 2301.

Dickinson, M.H., Lehmann, F.-O., Sane, S.P., 1999. Wing rotation and the aerodynamic basis of insect flight. Science 284 (5422), 1954.

Digby, P.S.B., 1958. Flight activity in the blowfly Calliphora Erythrocephala, in relation to light and radiant heat, with special reference to adaptation. J. Exp. Biol. 35, 1), 1.

Dixon, A.F.G., Mercer, D.R., 1983. Flight behaviour in the sycamore aphid: factors affecting take-off. Entomologia Experimentalis Et Applicata. 33 (1), 43.

Dudley, R., 2002. The Biomechanics of Insect Flight: Form, Function, Evolution. NJ, US. Princeton University Press Princeton.

Ellington, C.P., van, d.B., Willmott, A.P., Thomas, A.L.R., 1996. Leading-edge vortices in insect flight. Nature. 384 (6610), 626.

Ennos, A.R., 1988. The inertial cause of wing rotation in *Diptera*. J. Exp. Biol. 140 (1), 161.

Ennos, A.R., 1995. Mechanical behaviour in torsion of insect wings, blades of grass and other cambered structures. Proc. R. Soc. Lond. B Biol. Sci. 259 (1354), 15.

Faruque, I., Humbert, J.S., 2010. Dipteran insect flight dynamics. Part 1: longitudinal motion about hover. J. Theor. Biol. 264 (2), 538.

Hedrick, T.L., 2008. Software techniques for two- and three-dimensional kinematic measurements of biological and biomimetic systems. Bioinspiration Biomimetics 3 (3), 34001.

Kennedy, J.S., 1939. The behaviour of the desert locust (*Schistocerca gregaria (Forsk.)*) (Orthopt.) in an outbreak center. Trans. R. Entomol. Soc. London 89 (10), 385.

Khelifa, R., Zebsa, R., Amari, H., Mellal, M., 2013. Does Wind Affect Emergence Site Selection in *Odonata*? 21383–387.

Klassen, W., Hocking, B., 1964. The influence of a deep river valley system on the dispersal of Aedes mosquitos. Bull. Entomol. Res. 55 (02), 289.

Lehmann, F.-O., Dickinson, M.H., 1998. The control of wing kinematics and flight forces in fruit flies (*Drosophila spp.*). J. Exp. Biol. 201 (3), 385.

Lehmann, F.-O., Gorb, S., Nasir, N., Schützner, P., 2011. Elastic deformation and energy loss of flapping fly wings. J. Exp. Biol. 214 (17), 2949.

Lehmann, F.O., Schützner, P., Wang, H., 2013. Visual Motion Sensing and Flight Path Control in Flies.

Lin, T., Zheng, L., Hedrick, T., Mittal, R., 2012. The significance of moment-of-inertia variation in flight manoeuvres of butterflies. Bioinspiration Biomimetics 7 (4), 044002.

Mountcastle, A., Daniel, T., 2009. Aerodynamic and functional consequences of wing compliance. Exp. Fluids 46 (5), 873.

Murty, U.S., Mutheneni, S.R., Arunachalam, N., 2010. The effects of climatic factors on the distribution and abundance of Japanese encephalitis vectors in Kurnool district of Andhra Pradesh, India. J. Vector Borne Dis.. 47 (1), 26–32.

Nasir, N., Mat, S., 2019. An automated visual tracking measurement for quantifying wing and body motion of free-flying houseflies. Measurement. 143267–143275.

Pass, G., 2018. Beyond aerodynamics: the critical roles of the circulatory and tracheal systems in maintaining insect wing functionality. Arthropod Struct. Dev. 47 (4), 391–407.

Pennycuick, C.J., 1960. Gliding flight of the fulmar petrel. J. Exp. Biol. 37 (2), 330.

Pennycuick, C.J., 1968. A wind-tunnel study of gliding flight in the pigeon Columba Livia. J. Exp. Biol. 49 (3), 509.

Purse, V.B., Thompson, J.D., 2003. Emergence of the damselflies, Coenagrion mercuriale and Ceriagrion tenellum (*Odonata: Coenagrionidae*), at their northern range margins, in Britain. Eur. J. Entomol. 100 (1), 93–99.

Ravi, S., Crall, J.D., Fisher, A., Combes, S.A., 2013. Rolling with the flow: bumblebees flying in unsteady wakes. J. Exp. Biol. 216 (22), 4299.

Ricklefs, R., Miller, G., 1999. Ecology. 4 W. H. Freeman.

Schützner, P., 2016. Time-Resolved Analysis of Wing and Body Kinematics in Freely Maneuvering Wild-Type and Transgenic Fruit Flies Drosophila [Dissertation]. Doctor of Philosophy (PhD). Institute of Neurobiology, University of Ulm, Germany.

Stark, W., Johnson, M.A., 1980. Microspectrophotometry of *Drosophila* visual pigments: determinations of conversion efficiency in R1-6 receptors. J. Comp. Physiol. 140 (4), 275.

Stuart, A.M., 1958. The efficiency of adaptive structures in the nymph of Rhithrogena Semicolorata (Curtis) (*Ephemeroptera*). J. Exp. Biol. 35 (1), 27.

Vance, J.T., Faruque, I., Humbert, J.S., 2013. Kinematic strategies for mitigating gust perturbations in insects. Bioinspiration Biomimetics 8 (1), 016004.

Vogel, S., 1966. Flight in *Drosophila*. J. Exp. Biol. 44 (3), 567.

Wang, H., Zeng, L., Liu, H., Yin, C., 2003. Measuring wing kinematics, flight trajectory and body attitude during forward flight and turning maneuvers in dragonflies. J. Exp. Biol. 206 (4), 745.

Washburn, J.O., Washburn, L., 1984. Active aerial dispersal of minute wingless arthropods: exploitation of boundary-layer velocity gradients. Science. 223 (4640), 1088.

Weimerskirch, H., Martin, J., Clerquin, Y., Alexandre, P., Jiraskova, S., 2001. Energy saving in flight formation. Nature. 413 (6857), 697.

White, F., 2006. Viscous Fluid Flow. McGraw-Hill Higher Education.

Withers, T., Harris, M., 1997. Influence of wind on hessian Fly (Diptera: Cecidomyiidae) flight and egglaying behavior. Environ. Entomol. 26 (2), 327–333.

Yanoviak, S.P., Munk, Y., Kaspari, M., Dudley, R., 2010. Aerial manoeuvrability in wingless gliding ants (*Cephalotes atratus*). Proc. R. Soc. Lond. B Biol. Sci. 277 (1691), 2199.

Yorozu, S., Wong, A., Fischer, B.J., Dankert, H., Kernan, M.J., Kamikouchi, A., Ito, K., Anderson, D.J., 2009. Distinct sensory representations of wind and near-field sound in the *Drosophila* brain. Nature. 458 (7235), 201.

Zhang, Y., Sun, M., 2010. Dynamic flight stability of a hovering model insect: lateral motion. Acta Mech. Sinica 26 (2), 175.